



Society of Petroleum Engineers

SPE-187349-MS

High Pressure Tertiary-CO₂ Flooding in a Fractured Chalk Reservoir

M. Ghasemi and W. Astutik, Petrostreamz; S. Alavian and C. H. Whitson, Pera A/S; L. Sigalas and D. Olsen, Geological Survey of Denmark and Greenland; V. S. Suicmez, Maersk Oil and Gas A/S

Copyright 2017, Society of Petroleum Engineers

This paper was prepared for presentation at the SPE Annual Technical Conference and Exhibition held in San Antonio, Texas, USA, 9-11 October 2017.

This paper was selected for presentation by an SPE program committee following review of information contained in an abstract submitted by the author(s). Contents of the paper have not been reviewed by the Society of Petroleum Engineers and are subject to correction by the author(s). The material does not necessarily reflect any position of the Society of Petroleum Engineers, its officers, or members. Electronic reproduction, distribution, or storage of any part of this paper without the written consent of the Society of Petroleum Engineers is prohibited. Permission to reproduce in print is restricted to an abstract of not more than 300 words; illustrations may not be copied. The abstract must contain conspicuous acknowledgment of SPE copyright.

Abstract

The purpose of this study is to present the numerical and experimental evaluation of the tertiary-CO₂ flooding (CF) at high operating pressure and reservoir temperature. In this study, water flooding is followed by CO₂ injection into an outcrop chalk core with a centralized fracture. Our validated numerical models reproduce the result of core flooding experiments. In addition, we upscale the simulation model and investigate the scale dependency of the diffusion mechanism in a larger matrix-fracture domain.

The experiments used an outcrop core which is vertically placed in the core-holder with the total length of 28 cm and the diameter of 12.3 cm. The axial "fracture" is represented by a centralized hole with the diameter of 2.2 cm. We utilize the Wood's Metal technique to initially saturate the chalk core with the North-Sea-Chalk-Field (NSCF) live oil. The core sample is aged to restore the chalk wettability at the operating conditions. Then, the water flooding (WF) is performed by injecting brine from the bottom of the fracture and producing the oil from the top. After no additional produced oil is observed, the WF is stopped. A "shut-in" period follows, which allows preparing the rig for tertiary-CO₂ flooding. CO₂ is then injected from the top and the hydrocarbon streams are produced from the bottom of the fracture. The whole core flooding is operated at constant reservoir conditions at 300 bara (4351 psia) and 110 °C, which is higher than the typical NSCF reservoir conditions (258 bara and 110 °C). This allows us to investigate the efficiency of the tertiary-CF at a higher operating pressure condition.

We employ a compositional reservoir simulation with a developed equation of state (EOS) to model the experiment. An automated history matching procedure is developed to match the experimental results. The modeling workflow is capable of taking into account the significant vaporization effect observed during CF when the rich-CO₂ enters the three-phase separator. An upscaling study is conducted to evaluate the performance of CF in a single and multiple fracture-matrix systems. Moreover, the accuracy of dual porosity models is tested against the reference single porosity model.

We accurately model the WF experiment through tuning the oil-water capillary pressure and relative permeability data. The numerical model is capable of reproducing the CF lab results by employing the best match multi-component diffusion coefficients. Moreover, we successfully model the excessive water production during CO₂ injection by taking into account the hysteresis effect in water-oil capillary pressure and relative permeability.

Comparing these results with our previous work at lower reservoir pressure shows the positive effect of pressure on increasing the efficiency of the tertiary-CF in recovering more oil from a matrix-fracture system. Also, the tuned capillary pressure and relative permeability during WF indicate an active imbibition drive and a strongly water-wet system.

In the upscaling work, we consider the effect of several key parameters on oil recovery; e.g. matrix block size, fracture spacing, CO₂ injection rate, gravity drainage, vaporization and the diffusion. The results show that the mass transport is mainly dominated by diffusion in the lab scale even though this is not the case in the large matrix block size.

Our findings are an important step towards modeling the tertiary-CO₂ flooding in an actual fracture-chalk system. We also provide some important inputs that are necessary for upscaling tertiary-CF from a lab-scale into a field-scale reservoir model.

Introduction

CO₂ injection has proved its efficiency for enhanced oil recovery (EOR) in various field projects and pilot tests. In total, 79 CO₂-EOR projects were active worldwide in 2004. Among them, 71 projects were conducted in US, five immiscible CO₂-EOR pilots in Trinidad, two miscible CO₂-EOR in Canada and one commercial CO₂-EOR project in Middle East (Tzimas et al. 2005). Enick et al. (2013) report that more than 110 field projects in US, 60% of which are in Permian Basin in Texas, are active under CO₂ injection. CO₂-EOR has increased in US steadily since 1980 and contributes to more than 30% US oil production from all EOR methods (Tzimas et al. 2005).

Many simulation and experimental studies have shown that the CO₂ injection can be a very efficient recovery technique for most of the fractured oil reservoirs (Bellveau et al. 1993, Jensen et al. 2000, Hoteit and Firoozabadi 2006, Alavian and Whitson 2010, Ghasemi et al. 2017a, Ghasemi et al. 2016b). This is achieved by means of immiscible- or miscible-CO₂ flooding at reservoir conditions. When reservoir pressure is low or the in situ oil composition contains high amounts of C₇₊ fractions, the miscibility may not be developed between CO₂ and the reservoir oil. In such cases, the immiscible-CO₂ injection can still increase the oil recovery. For example, Tzimas et al. 2005 report a commercially successful immiscible CO₂-EOR in Turkey. The reservoir contains heavy-oil with low°API (9-15) gravity. It is estimated that 6.5% of original-oil-in-place (OOIP) was recovered by immiscible-CO₂ EOR. The improvement in oil recovery in immiscible CO₂ displacement is achieved through swelling of CO₂ into oil and decreasing the oil viscosity and hence improving the oil mobility toward the producer. CO₂ can vaporize the light-to-medium components and decrease the trapped oil saturation. Unlike the conventional oil reservoirs, diffusion can be a very efficient process in naturally fractured reservoirs with high fracture density, improving the oil recovery during active immiscible-CO₂ flood.

To achieve the first contact miscibility for CO₂-EOR, the pressure must be above the cricondenbar in p-x diagram which is beyond the limit for typical range of reservoir pressures. For example, our analysis shows the first-contact miscibility for CO₂ and the NSCF live-oil mixture at reservoir temperature may be achieved at elevated pressures above 20,000 psia. However, for the same mixture, the multi-contact condensing-vaporizing miscibility is achieved at a minimum miscibility pressure (MMP) of ~3000 psia. The residual oil saturation may reach close to zero under miscible displacement. For example, the oil recovery in 1D miscible displacement should be almost 100% after one pore-volume (PV) of the injected displacing fluid. However, the performance often drops in highly heterogeneous reservoirs because of poor sweep efficiency, which may not be the case for the naturally fractured reservoirs. Firoozabadi and Markeset (1994) conduct miscible displacement experiments for several matrix-fracture configurations. They conclude that miscible displacement in fracture reservoirs can be an extremely efficient process. In miscible CO₂ flooding, the oil recovery is improved through swelling the matrix oil, decreasing oil viscosity and eliminating the gas-oil

interfacial tension (IFT) at the miscible front in the matrix. In addition, diffusion, dispersion and dissolution of the injected CO₂ play a considerable role in the mass transfer between matrix and fracture (Hoteit and Firoozabadi 2006, Ghedan 2009, Moortgat et al. 2013).

However, there are certain concerns and challenges in the applicability of the CO₂-EOR project in onshore and offshore fields (Tzimas et al. 2005, Goodyear et al. 2011): (a) the remaining oil saturation after water-flooding should be sufficiently high 35-40%, (b) fracture-matrix interactions at larger scale, (c) for miscible CO₂-EOR, the oil gravity should be higher than API of 35° and the operation above MMP should not be a field constraint (Tzimas et al. 2005), (d) injectivity may reduce due to precipitation of asphaltene and hydrate near the wellbore, (e) formation of scale in the water pipeline and wells (f) during tertiary CO₂-EOR, the large fluid separation and compression unit is needed to handle the excessive water production and produced CO₂ from the reservoir (g) the CO₂ supply. Moreover, many research and studies have been conducted to increase the efficiency of the CO₂-EOR by means of CO₂-WAG (water-alternative-gas), CO₂-foam and the CO₂-chemical flooding (Jensen et al. 2000, Enick et al. 2013, Awan et al. 2006, Zuta et al. 2010).

Certainly, for fracture system, it is essential to study the tertiary-CO₂ EOR in lab scale before moving to field or to a pilot test. This helps to understand the complex displacement mechanisms and the interaction between the matrix and the surrounding fracture. Therefore, a series of experiments and simulations have been conducted to achieve a better insight of the tertiary-CO₂ process in a fractured reservoir (Ghasemi et al. 2016b, Ghasemi et al. 2017a, Ghasemi et al. 2017b). Ghasemi et al. (2017a) perform an extensive experimental and simulation work of tertiary CO₂ injection into a large fractured-chalk core. The core sample is 26 cm long and 12 cm in diameter. In their work, one experiment is carried out at reservoir condition employing the NSCF live oil. Results show high oil recovery (~75%) after water flooding, indicating an active water imbibition between fracture and matrix. The tertiary-CF could increase the oil recovery by few percentages. They conduct the experiment at reservoir pressure of 258 bara (3750 psia) and 110 °C.

We present the experimental and simulation study of the tertiary-CO₂ EOR in a similar size core and fracture aperture as being used by Ghasemi et al. (2017a). The main difference is that the experiment is conducted at a higher reservoir pressure of 300 bara (4350 psia). This allows us to study the efficiency of the CO₂-EOR at different reservoir pressures. To the best of our knowledge, such measurements and modeling work to investigate effect of pressure on the CO₂-EOR performance in a fractured-chalk has not been performed earlier.

Once the experimental work and the history-matching are performed, we go one step further and upscale the results into a larger scale. Upscaling allows us to identify the role of the diffusion and convective flow at different matrix-fracture domain by considering the key parameters that affect the applicability of the CO₂-EOR in the field scale. Some important input parameters for the upscaling work are provided by our studies at the core-scale such as the diffusion coefficients, capillary pressures and relative permeabilities. We also study the accuracy of dual porosity models against the reference single porosity model by testing different transport functions under tertiary-CO₂ EOR process.

The paper is arranged as follows: First, we present the results of an experiment conducted at high pressure and temperature conditions. We describe the history matching procedure which is used to verify our numerical model. We then compare our findings with a previously conducted experiment at same temperature but at lower pressure. Afterwards, we provide a discussion on the upscaling procedure and demonstrate the results obtained on a number of sensitivity studies by altering the fracture spacing, matrix block height, injection gas and transfer functions utilized in dual permeability modelling. We then complete the paper with our observations and concluding remarks.

Experimental Descriptions

This section provides a complete description of the core material used in the experiment, the fluid properties, the experimental preparations, and the core flooding procedures.

The Core Material

The experiment is conducted at high reservoir pressure and reservoir temperature with an outcrop chalk sample from the Tor formation of the Sigerslev Quarry, in Stevns Klint, Denmark, as an analog for NSCF rocks. We take special consideration for selecting the best candidate chalk cores in terms of the high degree of homogeneity. We run X-ray computed-tomography (CT) scanning tests for various chalk-core plugs before selecting the best candidate cores. Fig. 1a shows the longitudinal image of the chalk core sample being used in the experiment. The average permeability of the chalk sample is estimated to be between 3.2 and 4.1 md. The measured average porosity is 46.8%.

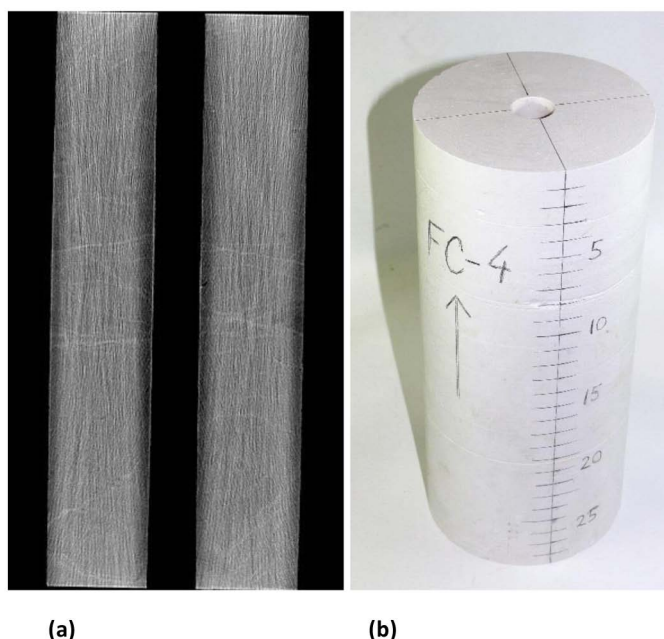


Figure 1—(a) The core plug's longitudinal CT scanned-images, (b) The chalk sample used for high pressure experiment (note the fully open axial hole).

Fluid Properties

We developed the NSCF fluid characterization and the EOS model based on available PVT data. The PVT data used in our EOS development studies are: standard depletion type experiments (CCE, DLE and separator tests), vaporization study, MMP measurements, and oil swelling test as a function of dissolved CO_2 . The EOS model is further reduced to 10 components; including 4 pseudo-fractions ranging from C_7 to C_{36+} . The EOS is referred to as EOS10. We perform this experiment using the NSCF live oil sample. The saturation pressure of the sample is found to be 251.8 bara at reservoir temperature of 110 °C. For tertiary- CO_2 experiments, it's important to have proper estimation of the interfacial tension between oil and gas phase to update the gas-oil capillary pressure. Therefore, we perform series of IFT experiments at several elevated pressures and different CO_2 mixtures. We observe a considerable decrease of IFT from 12.2 mN/m at 61 bara to 1.0 mN/m at 253 bara. The IFT measurements are matched with the EOS10 by tuning the EOS's Parachor of the C_{7+} and CO_2 components. The EOS10 is then utilized by our developed numerical model to provide an accurate volumetric and phase properties of various oil- CO_2 mixtures at reservoir conditions (Appendix A).

We employ the DUC EOR sea water with similar salinity as the North Sea for the injected brine and for establishing the initial formation water. The brine has considerable amount of sulphate (2780 mg/L) that is found to be the main cause for developing a strong imbibition drive during water injection (Ghasemi et al., 2017b).

Experimental Preparation

In this experiment, the outcrop chalk sample is placed vertically inside the core holder with the total length of 27.8 cm and the diameter of 12.3 cm. We drill a 2.2 cm centralized axial hole in the chalk sample that represents the "fracture". The current matrix-fracture configuration has a pore-to-fracture volume ratio of 14. The selected chalk sample in this experiment was taken adjacent to the sample used in the recent work of [Ghasemi et al. \(2017a\)](#) and has similar dimensions. This allows us to study the effect of system pressure on the performance of tertiary- CO_2 injection in a fracture-matrix system. The schematic of the selected chalk sample is illustrated in [Fig. 1b](#).

Initially, we saturate the chalk core with DUC EOR sea water. Then the sample is saturated to $S_o=85\%$ with NSCF stock tank oil (STO) using the evaporation technique of [Springer and Korsbech \(2003\)](#). In order to allow replacement of the STO within the pore space of the sample with the live oil, the axial fracture of the core sample is sealed with Wood's Metal. After that, the core sample is wrapped in metal foil, enclosed in a rubber sleeve, and mounted in a hydrostatic core holder. The rubber sleeve and the metal foil prevent mass transfer between the core sample and the core holder annulus during the flooding experiments. The core holder with the core sample is then mounted in the experimental rig with a vertical orientation, and a net overburden pressure (NOB) of 14 bar is applied. Conditions of $P=300$ barg (4351 psia) and $T=65$ deg C are established. The temperature is kept below the melting point of Wood's Metal, which is 70 degree C. STO in the core sample is replaced with NSCF live oil by flushing the live oil through the core, while the axial fracture is sealed. The rig is equipped with a densitometer in the flowline downstream to the core holder that records the density of the oil produced from the core. When the recorded fluid density is constant and close to the density of pure live oil, the exchange process is complete. The density of pure live oil was determined by flowing live oil directly to the densitometer through a flowline that bypassed the core sample. The rig temperature is then raised to 110 degree C and the Wood's Metal is flushed downwards out of the axial fracture into a waste container below the core sample. Inspection of the core sample and the connected flowlines after the experiment revealed virtually no residual Wood's Metal. The technique of Wood's metal is previously used by [Ghasemi et al. \(2017a\)](#) and [Karimaie \(2009\)](#). Afterwards, the ageing process starts and lasts for 28 days to equilibrate the rig and restore the reservoir wettability. The whole rig components are remotely controlled via integrate computer that controls the core flooding experiments as well as provide the preliminary data of flow rate, cumulative amount of produced oil, gas and water, density profile, temperature profile, and the system pressures. Note that the whole core flooding experiments are operated at constant reservoir temperature.

Water Injection

After ageing the chalk sample at high reservoir pressure of 300 bara (4351 psia) and the reservoir temperature of 110 °C, the WF starts by injecting water from the bottom of the centralized fracture. The streams of oil and water are produced from the top of the fracture. The live-oil at the mentioned condition is single phase and separates into gas and oil phases in the three phase separator operated at the 4 bara and at 24 °C. WF lasts for the 453.9 hours ($PV_{inj}=3.2$). When we observe no-more oil is recovered from the chalk sample, the water flooding is stopped and the shut-in period starts by isolating the core holder from the separator. The shut-in period allows us to prepare the rig for CO_2 injection and ended after 97.5 hours.

We observe a strong imbibition drive and strongly water-wet behavior during the water flooding experiment. A similar observation is also reported by [Ghasemi et al. \(2017a\)](#) in an earlier study. The oil breakthrough occurs at 72.5 hours ($PV_{inj}=0.609$) and results with a water saturation of 69.5 % at the breakthrough. The ultimate oil recovery is 67% which is quite high as compared to the typical value (~55%) reported for the NSCF chalk reservoirs ([Jensen et al. 2000](#)). The reason for developing the strong imbibition drive is discussed elsewhere ([Ghasemi et al. 2017a](#)).

CO₂ Injection

Right after the shut-in period, CF starts by injecting CO₂ to the top of the fracture. The flow direction is downward and the rich-CO₂ mixtures are produced from the bottom of the fracture. Right at the start of CO₂ injection, we observe sharp increase in oil production. The produced oil pocket is due to an active imbibition drive during shut-in period and is previously discussed by [Ghasemi et al. \(2017a\)](#). The CO₂ injection lasts for more than 200 hours, resulting in an ultimate oil recovery of 75.4 %, i.e. 8.4% incremental oil recovery is achieved for CO₂-PV_{inj}=2.4 during CF. The CO₂ at this condition acts as a super critical fluid with the density of 0.632 g/cm³. The whole operation during WF and CF is conducted at a constant reservoir pressure of 300 bara (4351 bara) with a negligible pressure gradient between the inlet and outlet which minimizes the impact of viscous forces on the displacement efficiency.

Compositional Modeling of the High-Pressure Tertiary-CF Test

A compositional finite-difference based simulator is employed to model the core flooding experiment at high operating pressure and reservoir temperature. We utilize ECLIPSE 300 (version 2012.1) in fully implicit mode during all our simulations. The detailed description is as follows:

Compositional Model Properties

A 2D x-z numerical model is developed to mimic the core flooding experiment in a matrix-fracture system. The model is represented by two regions with distinctive properties. Region one contains the fracture grids and is characterized by assigning high fracture permeability and 100% porosity. The Region two presents the matrix grids with the chalk porosity of 46.8% and klinkenberg permeability of 4 md. [Table 1](#) provides the physical properties of Region 1 and Region 2 as well as the optimum grid block dimensions. The mass exchange takes place between matrix and fracture and the mass-flow inlet and outlet are only allowed through Region 1. Similar with experiment, at initial conditions we initialize the fracture with 100% live-oil and the matrix with 85% live-oil and 15% connate water saturation. The model is operated under constant pressure of 300 bara and temperature of 110 C. The separator condition is set to 4 bara and 24 °C.

TABLE 1—ROCK AND FLUID ROPERTIES AS WELL AS SYSTEM DIMENSIONS USED IN THIS WORK

	High-Pressure Experiment	
	Fracture	Matrix
Initial System Pressure, bara	300	300
Temperature, °C	110	110
Ave. Porosity, %	100	46.8
Ave. Permeability, md	2000	4.1
Total Length, cm	27.85	27.85
Diameter, cm	2.243	12.309*
PV, cm ³	110.04	1498.46
Initial Oil Density**, g/cm ³	-	0.708
CO ₂ Density**, g/cm ³	0.632	0.632
Grid Dimensions in x-dir, cm	1.12	0.125825
Grid Dimensions in z-dir, cm	1.11396	1.11396
Number of grid in x-dir	1	40
Number of grid in z-dir	25	25
Initial Oil Saturation, %	100	85
Initial Water Saturation, %	0	15
Oil Type	Live Oil NSCF	
Rock Type	Outcrop	
Brine Viscosity**, cp	0.283	
Brine Formation Factor, cm ³ /cm ³	1.0359	
Separator pressure, bara	4.0	
Separator temperature, °C	24	
* sample diameter includes both matrix and fracture.		
** at reservoir conditions.		

We measure the gas-oil capillary pressure of the chalk core by means of mercury injection experiment in the lab (Ghasemi et al. 2016b). However, we assigned a linear gas-oil relative permeability to Region 2. The assumption of linear relative permeability is reasonable since we do not observe a significant effect of gas-oil relative permeability on the performance of tertiary-CO₂ flooding. We assign linear relative permeability and zero capillary pressure to Region 1. da Silva (1989) reports the water-oil relative permeability (k_{row}) and capillary pressure (P_{cow}) for NSCF chalk reservoirs which are utilized as the base case data in our modeling. However, the k_{row} and P_{cow} are found to have a significant effect on the performance of the water injection and are tuned during model validation process.

The two well pairs are defined in our numerical model. The first well-pair is active during WF in which the injector is under a constant injection rate of 12 cm³/hour and later changed to 7.5 cm³/hour. And the producer is under constant pressure constraint. The first well-pair is shut in at the end of WF and the second well-pair is active during CF. Similar rate and pressure constrains are applied to producer and injector during CF period.

Finally, Ghasemi et al. (2017a) provide the detailed procedures on the history matching of the WF and CF process. In their procedure, the model is integrated with the modified water-oil capillary pressure correlation to match the reservoir performance in WF period. The model is updated each time with based on n_I , n_F and

S_{wt} values. n_I and n_F are the tuning parameters that control the shape of the water-oil capillary pressure in spontaneous- and forced imbibition respectively. The S_{wt} is a water saturation point where the spontaneous imbibition changed into forced-imbibition drive. During CF, history matching procedure involves tuning diffusion coefficients, hysteresis effect on the water-oil capillary pressure and relative permeabilities. We provide further discussion in the proceeding sections.

Matching the Experimental Results

We inject 4813.4 cm^3 ($PV_{inj}=3.2$) of water at reservoir conditions. High oil recovery after secondary water flooding represents strong water-wet system and a significant spontaneous imbibition during WF. The history matching procedure for WF period is previously described by [Ghasemi et al. 2017a](#). As shown in [Fig. 2a](#), we found the best match capillary pressure and relative permeability that provide the good fit to the WF data. As shown by [Fig. 2b](#), the resulted capillary pressure is slightly different than that was found by [Ghasemi et al. 2017a](#), representing a slightly less water wet system. The final water saturation found in this work is 71.9% which is slightly lower as compared to $S_w=75\%$ reported by [Ghasemi et al. \(2017a\)](#).

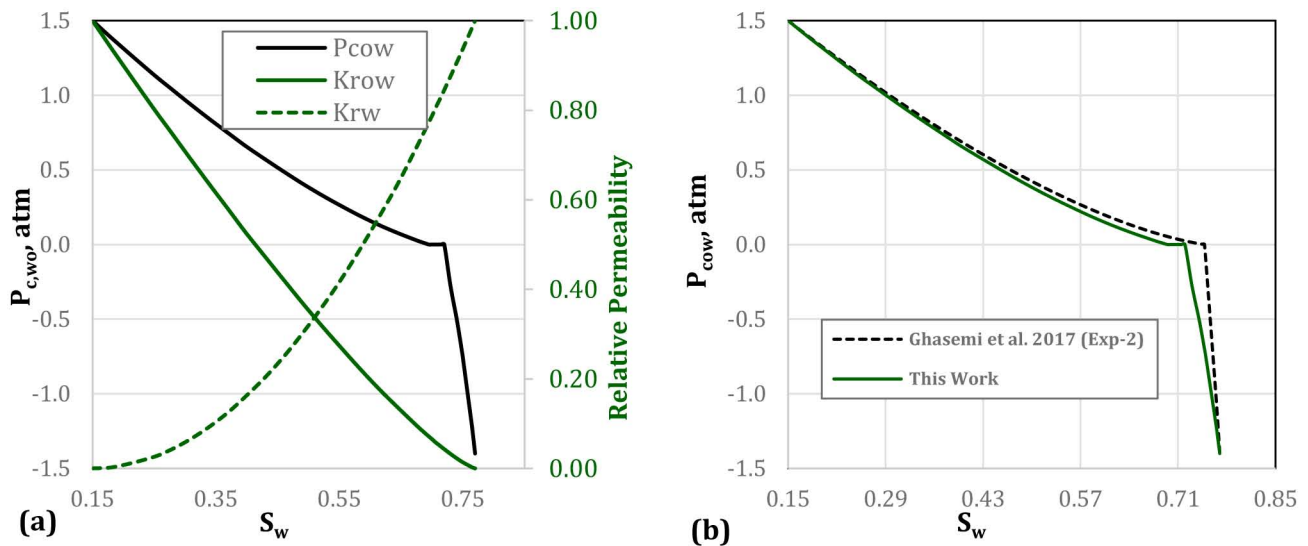


Figure 2—Capillary pressure and relative permeability: (a) the best match capillary pressure and relative permeability, (b) The best match of P_{cow} used in this work and [Ghasemi et al. \(2017a\)](#)'s work.

[Fig. 3](#) presents the good match obtained for cumulative oil at reservoir condition and the water production at surface conditions. The break through time is well predicted by the model.

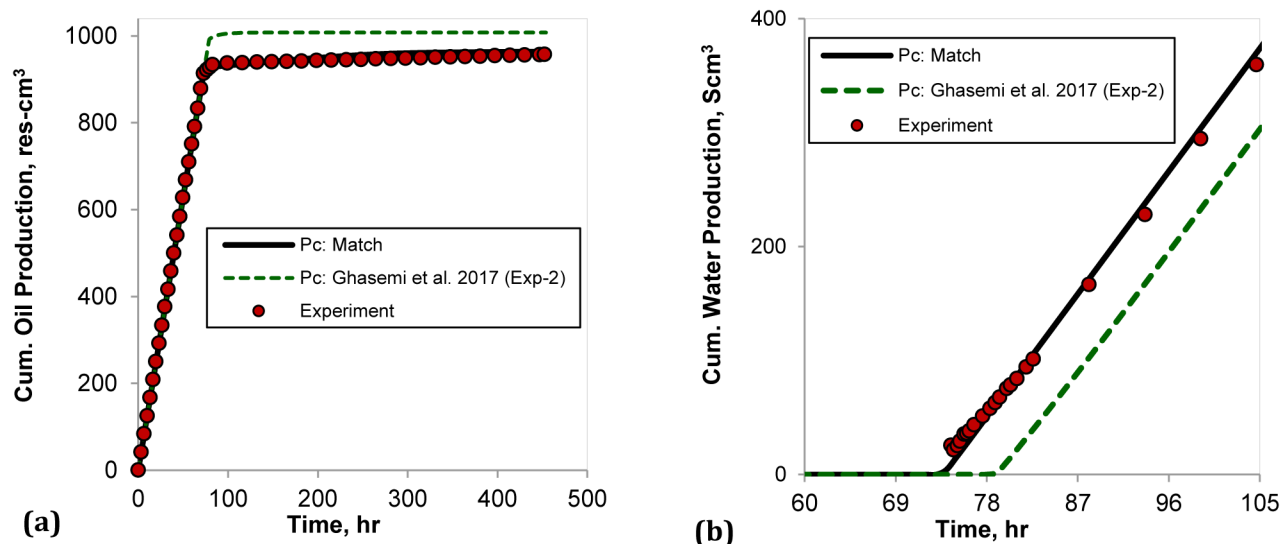


Figure 3—Effect of oil-water capillary pressure: (a) cumulative oil production at reservoir condition, (b) cumulative water production.

Using P_{cow} found by Ghasemi et al. (2017a)'s work results in higher oil production after water break through. Moreover, the water break through is slightly over predicted, indicating higher spontaneous imbibition using the P_{cow} by Ghasemi et al. (2017a).

However, the cumulative oil and gas production at surface conditions predicted by the tuned model are found to be significantly over predicted. The main reason is also addressed by Ghasemi et al. (2017a) indicating the change in the PVT properties of the original live-oil during exchange process. PhazeComp (version 1.8.1) is employed to model the PVT behavior through the exchange process by using the EOS model provided in Appendix A. The regression results reveal that the oil remaining inside the core contains 7.89% original STO and 92.11% Live-Oil. This indicates a more efficient exchange process by use of Wood's Metal in this work as compared to our previous work (Ghasemi et al., 2017a), where the remaining oil in the core during the exchange process found to be more contaminated by STO (15.87% STO and 84.13% live-oil composition). Fig. 4 compares the final live-oil composition after the exchange process for this study and our previous work (Ghasemi et al., 2017a).

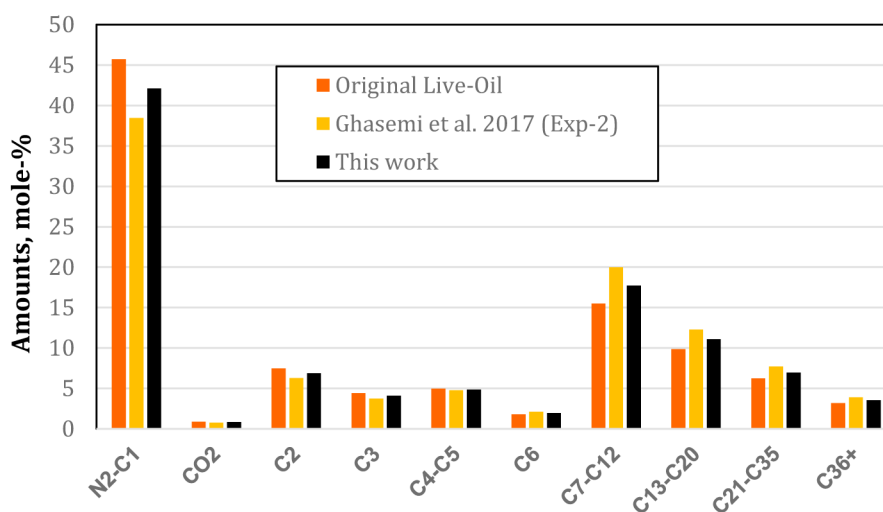


Figure 4—Change in oil composition during exchange process.

After initializing the numerical model with the newly established oil mixture, the oil and gas production data at surface conditions show a very good agreement with the experimental measurement (Fig. 5). It is worth mentioning that the reported oil production at surface conditions is corrected for vaporization effect during water flooding period.

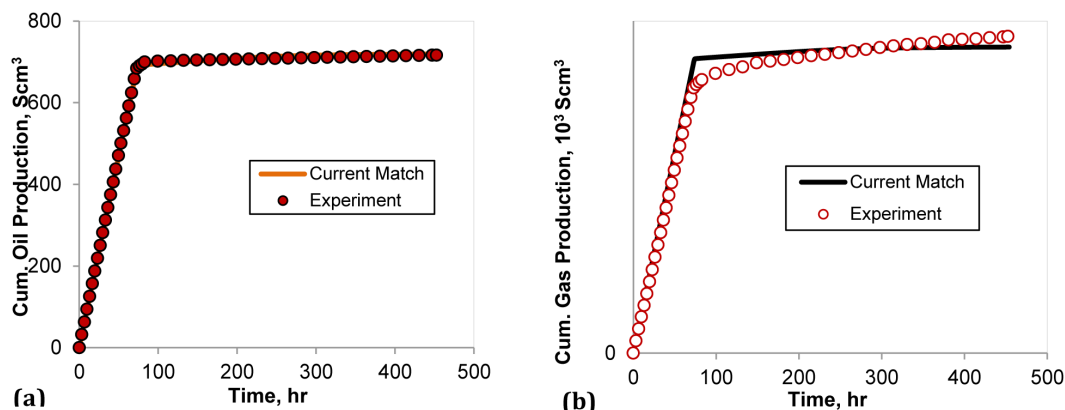


Figure 5—Quality of fit for this work during WF: (a) surface-cumulative oil production, (b) surface-cumulative gas production.

During CF, we observed the reduction of the surface oil production due to significant amount of vaporization caused by rich- CO_2 entering the separator. The CO_2 vaporizes the oil and extracts the light-to-medium components out of the separator. We collect the gas sample from separator and measure its compositions at several points during CO_2 injection. Ghasemi et al. (2017a) present the detailed description of the vaporization effect and provide the systematic procedure to correct the produced oil data at surface condition. Similar approach is used in this work. We also observe significant water production during CF which cannot be predicted by only tuning the diffusion coefficients (Fig. 6). To account for the additional water recovery, we modify the water-oil capillary pressure and relative permeabilities. We find considerable effect of hysteresis while matching the water production. Fig. 6 compares the model with and without hysteresis against the experimental data. The gray-dashed line represents the best match water production observed in the work by Ghasemi et al. (2017a). Water production data in this work shows the higher water production rate compared with that reported by Ghasemi et al. (2017a). The final hysteresis in oil relative permeability is found to be similar with Ghasemi et al. (2017a). However, the hysteresis in capillary pressure is different and is shown in Fig. 7.

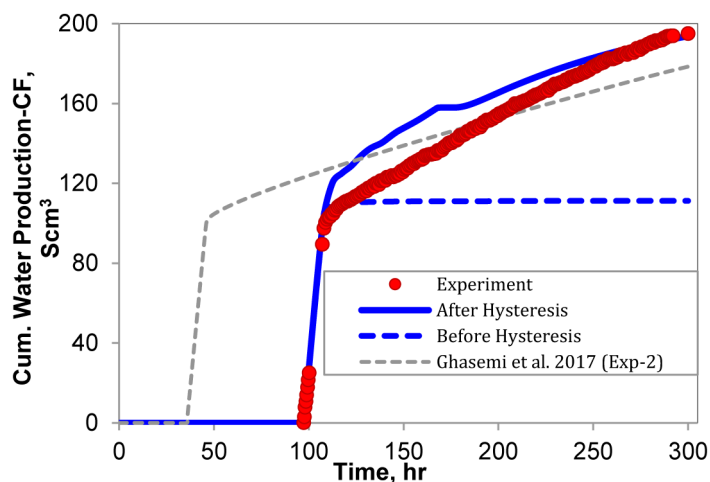


Figure 6—Effect of Hysteresis on the performance of water production during CF.

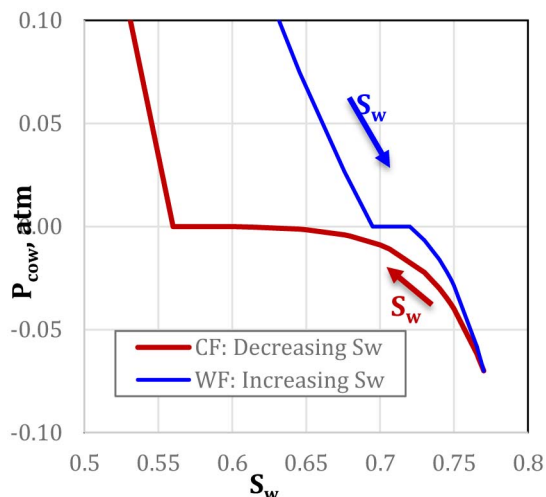


Figure 7—Hysteresis in oil-water capillary pressure during CF.

Finally, the best match oil production is obtained by tuning the diffusion coefficients during CF. We use similar history matching procedure presented by Ghasemi et al. (2016b) to estimate the two sets of diffusion coefficients during CO₂ injection. The reason is that diffusion coefficients may alter in time when the CO₂ content in oil increases.

Fig. 8 shows the strong dependency of the tertiary-CO₂ recovery on the diffusion coefficients. Similar to Ghasemi et al. (2017a)'s work, ignoring the dependency of diffusion coefficients to composition fails to provide good match against the experimental data. Table 2 provides the best match diffusion coefficients obtained during history matching. Fig. 8 shows the best match oil production data against the measured oil production during the CO₂ injection. Dashed line shows no oil recovery when diffusion is ignored revealing the important role of diffusion at high pressure and large fracture density. Moreover, it's the oil-like density of the super critical CO₂ at high pressure ($\rho_{CO_2}=0.632 \text{ g/cm}^3$, $\rho_{oil}=0.708 \text{ g/cm}^3$) dampen the positive role of gas-oil gravity drainage (GOGD) mechanism which heavily relies on the density difference.

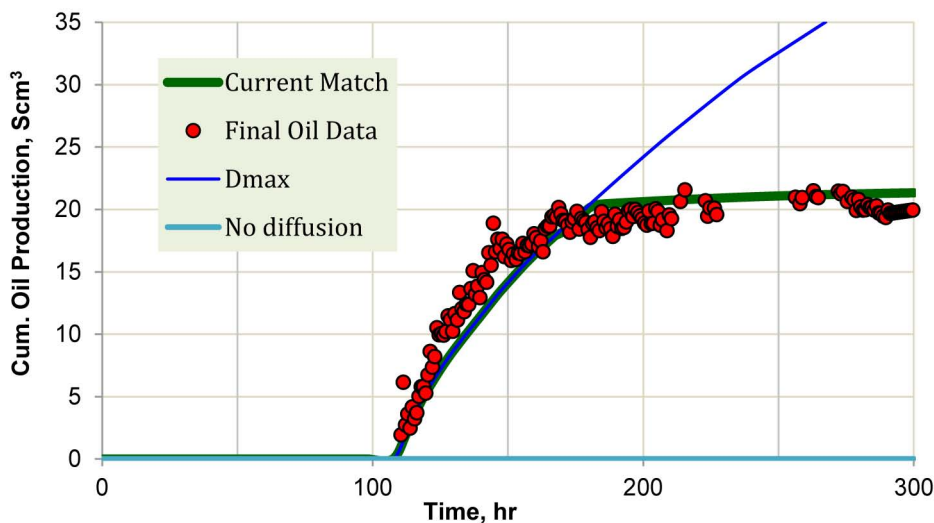


Figure 8—Effect of multi-components diffusion coefficients on the performance of tertiary-CO₂ recovery. Best match is shown with green line.

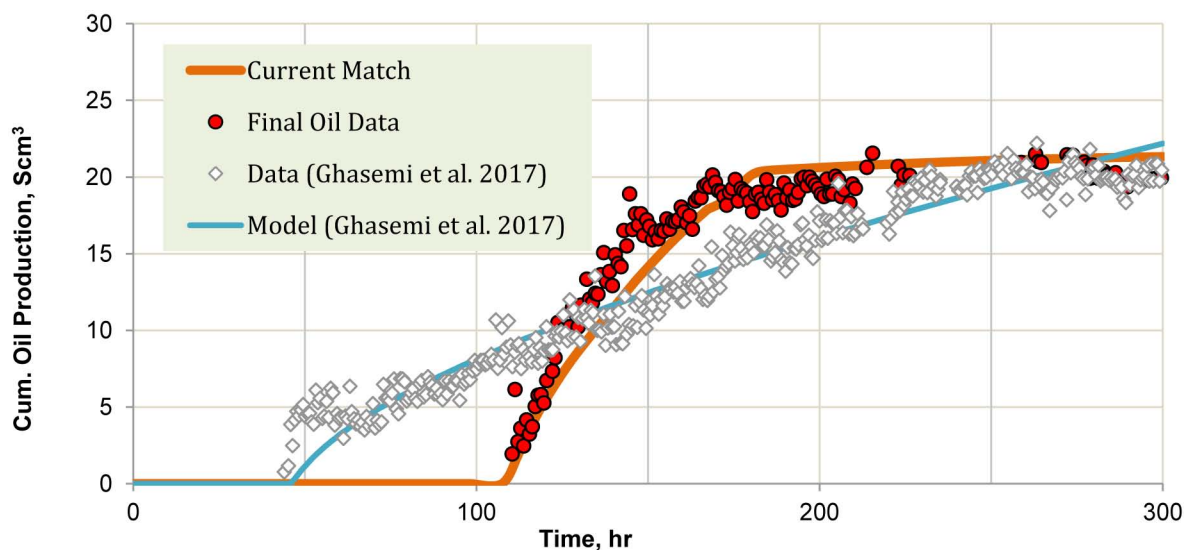
TABLE 2—THE BEST MATCH DIFFUSION COEFFICIENTS FOUND IN THIS WORK

	D_{io}^* , cm ² /hr	D_{ig}^* , cm ² /hr	D_{io}^{**} , cm ² /hr	D_{ig}^{**} , cm ² /h
N ₂ C ₁	3.206E-02	4.361E-01	3.16E-03	9.22E-04
CO ₂	3.023E-02	1.822E-01	9.85E-04	5.61E-04
C ₂	3.050E-02	2.869E-01	2.09E-03	7.09E-04
C ₃	2.410E-02	2.213E-01	1.61E-03	5.54E-04
C ₄ C ₅	1.911E-02	1.742E-01	1.26E-03	4.38E-04
C ₆	1.621E-02	1.472E-01	1.06E-03	3.70E-04
C ₇ C ₁₂	1.308E-02	1.108E-01	7.94E-04	2.96E-04
C ₁₃ C ₂₀	9.507E-03	7.531E-02	5.69E-04	2.09E-04
C ₂₁ C ₃₅	6.718E-03	5.055E-02	4.30E-04	1.45E-04
C ₃₆₊	5.095E-03	3.858E-02	4.03E-04	1.10E-04

* Best Match D_{io} and D_{ig} for 0-to-70 hours.
** Best Match D_{io} and D_{ig} for t>70 hours.

Performance of Tertiary CO₂ recovery at High Pressure

Ghasemi et al. (2017a) performed a similar experiment at the same temperature 110 °C and a lower pressure of 258 bara (3750 psia). We compare the results in Fig. 9. As can be seen, the performance of tertiary-CO₂ recovery at high pressure significantly increases. The oil production rate after the start of CF is considerably higher as compared to CF at lower pressure. The oil recovery at the end of CF reaches around 21Scm³.

Figure 9—Tertiary-CO₂ recovery for 255 and 300 bara systems.

Figs. 10 provides a detailed explanation for high efficiency of tertiary CO₂ recovery at high pressure system. As shown by Fig. 10a, the first contact miscibility is not achieved by CO₂ flooding into a NSCF-fracture oil reservoirs. However, the saturation pressure of the live-oil/CO₂ mixture is 300 bara after around 40% of CO₂ is injected. This means that the oil can dissolve around 40% of CO₂ without forming a gas phase at 300 bara as compared to only around 10% at 258 bara (Fig. 10b) which leads to significant viscosity

reduction in oil phase and hence results in higher rates of oil recovery. As pressure increases, the multi-component diffusion coefficients may decrease due to increase of molar density. However, oil diffusion coefficients, which has more considerable effect than the gas diffusion coefficients (Ghasemi et al., 2016a), remain almost the same at both pressures (Fig. 10c). Moreover, vaporization becomes more efficient at higher pressure as shown in Fig. 10d. Therefore, the performance of tertiary CO₂ recovery at high pressure is better as compared to the low pressure system.

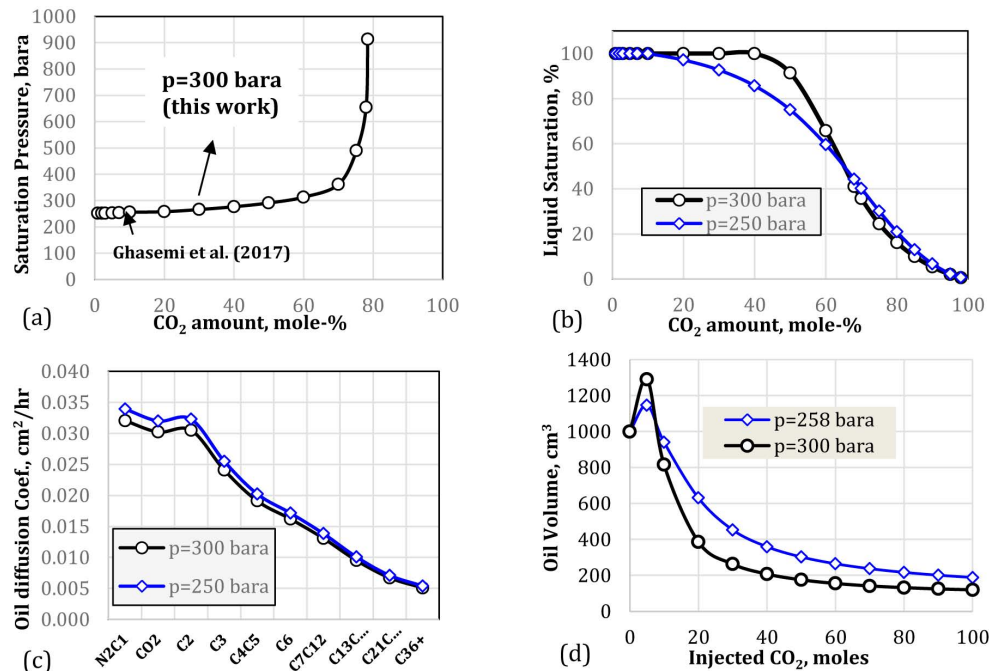


Figure 10—PVT dependent properties of CO₂/live-oil system at different operating conditions: (a) saturation pressure, (b) liquid saturation, (c) oil diffusion coefficients, and (d) vaporization at reservoir conditions.

Upscaling the CO₂-EOR

This section covers the upscaling of the secondary and tertiary CO₂ injection into a fracture-matrix system from lab to the field scale. It addresses the essential parameters in the larger scale that controls the rate of oil recovery and the efficiency of the process. The detailed description is given as follows:

Numerical Model Properties

In our study for field-scale matrix-fracture system, we utilize a single matrix surrounded by fracture to evaluate the mass transport mechanism and the oil recovery subjected to different injected gas. The initial fluid composition is the live-oil NSCF selected from the work of Ghasemi et al. (2016a). Fig. 11 summarizes the typical NSCF physical properties selected for upscaling work. The base case matrix is represented by a cube with 1-m dimensions, 35.7 % the porosity, and the isotropic permeability of 2 md. The matrix is surrounded by a fracture with typical aperture of 0.1 cm and fracture porosity and permeability of 100% and 5000 md. Because of the block symmetry, we model only the half of the matrix block. Fig. 11a provides the physical properties used in the upscaling. Fig. 11b shows the base case model with half of the matrix surrounded by one vertical fracture on the right edge of the matrix and two horizontal fracture at the top and bottom of the matrix block. The matrix is initially saturated with NSCF live-oil and the fractures are initialized with the injected gas.

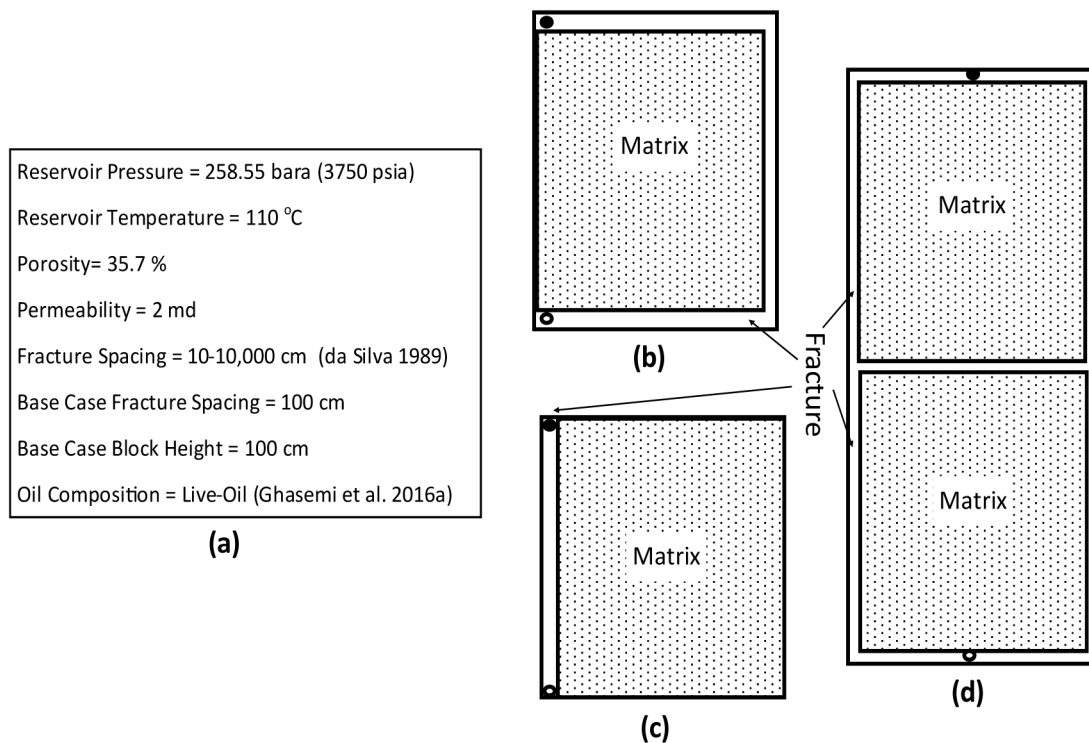


Figure 11—Schematic of numerical modeling considered for upscaling: (a) typical NSCF block properties, (b) matrix surrounded with three fractures, (c) single matrix and single fracture, (d) example of two stack matrix blocks.

We select the gas-oil capillary pressure from the work of [Ghasemi et al. \(2016a\)](#) and the linear relationship for the gas-oil relative permeability. The NSCF reservoir conditions defined in our model are 258.6 bara (3750 psia) and 110 °C. We place the injector at the top-left corner and the producer at the bottom-left corner ([Fig. 11b](#)). Injector is operated under rate control and the producer under the pressure control. Therefore, the system pressure is kept constant and we eliminate the effect of viscous forces in the fracture-matrix system. The base case injection rate is selected so that one injected PV equals 10 years of injection into a specific matrix-block dimensions. The oil and gas diffusion coefficients are selected from the results of constant volume diffusion tests conducted by [Ghasemi et al. \(2016a\)](#).

We develop an automated grid builder with higher resolution near the vertical and horizontal fractures and larger grids toward the no-flow boundaries. The inner grid-distance for each grid cells is geometrically spaced and equals the log mean of the grid-center distance of the current cell and the neighbored grid cell. Similarly, the total matrix length is the log mean of the grid-center distance of the last cells defined in the gridding system.

Oil Recovery Calculation

It is important to report the correct oil recovery subjected to different injection gas. If the produced stream is not corrected for the produced injected-gas, the resulted oil recovery may not correctly address the produced in situ oil. Therefore, (a) we first correct the produced stream from the produced injected-gas at each running time interval, (b) then, we flash the corrected stream at the separator condition. (c) the initial oil composition is flashed at the similar separator condition defined in b. (d) then the oil recovery is obtained by: $R_o\% = \sum V_{o,b}/V_{oi,d} \times 100$, where the $V_{o,b}$ is the resulted surface oil volume from step b and the $V_{oi,d}$ is the initial oil in place from step c.

Upscaling Results

This section describes the sensitivity analysis of some important parameters affecting the efficiency of the CO₂-EOR at the larger scale.

BaseCase Recovery Mechanism. The base case model is run to understand the role of diffusion for controlling the rate of mass transport between matrix and fracture. The model runs for 50 years ($PV_{inj}=5$) by injecting CO_2 at the top and producing the hydrocarbon streams from the bottom of the block. Fig. 12 compares the oil recovery after 5 PV of the injected CO_2 . The ultimate oil recovery for the case with diffusion is 83% while no-diffusion results in insignificant oil recovery as shown earlier in this study. It reveals the strong effect of diffusion for controlling the mass transport and the rate of oil recovery. For this dimensions ($1m \times 1m \times 1m$), the diffusion is dominant over gravity drainage. Later we discuss the effect of block height and fracture spacing.

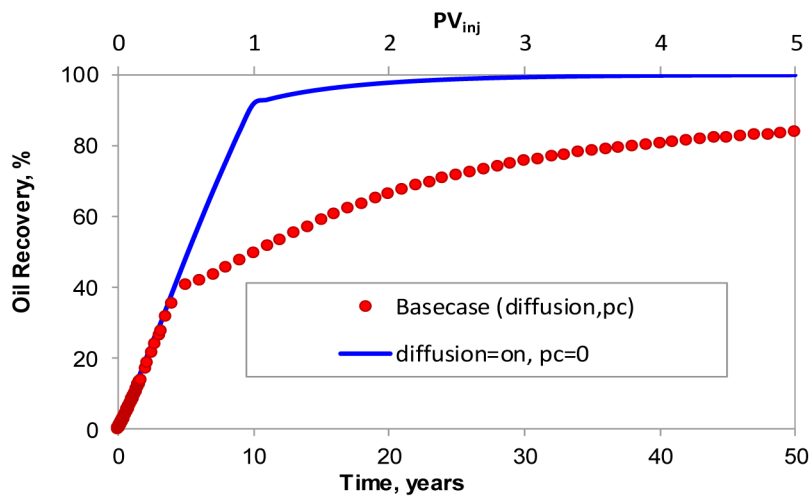


Figure 12—The profile of oil recovery after 50 years

As depicted by Fig. 13, the mass transport within the matrix is considerably affected by IFT variations. CO_2 enters from fracture into matrix mainly by means of diffusion, overcoming the capillary force from a region with low IFT. The oil is recovered less from those regions in the direction of the maximum IFT, and high P_{cgo} . The phase distribution inside the matrix changes for different sets of the gas-oil capillary pressure.

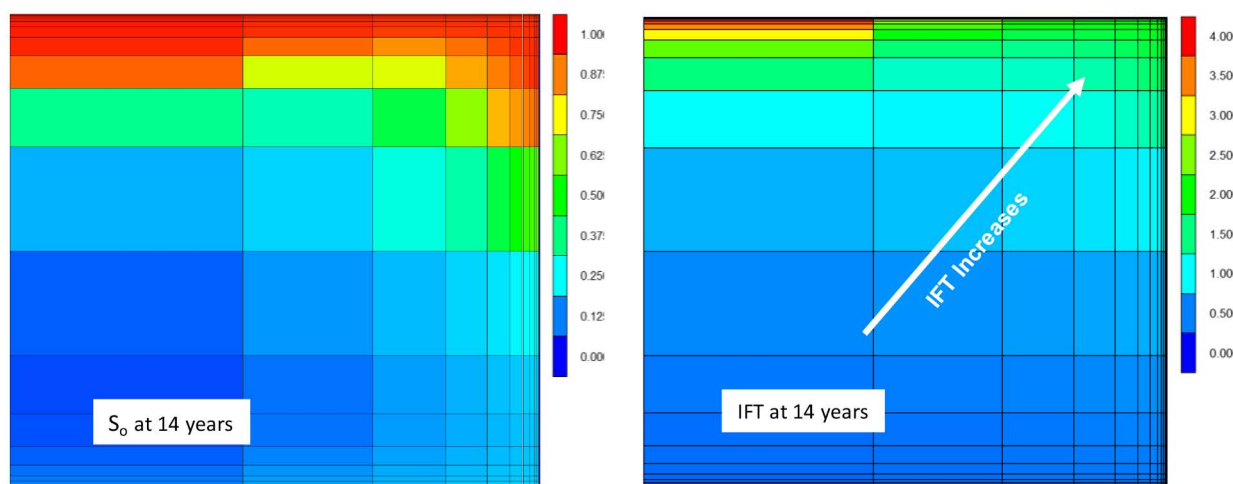


Figure 13—The snapshot of the oil saturation and IFT after 14 years shown for case b presented in Fig. 11

We run the base case with zero-capillary pressure. As shown in Fig. 12, neglecting capillary pressure leads to more than 90% oil recovery at $PV_{inj}=1$, and 100% oil recovery after 30 years ($PV_{inj}=3$). It develops the piston-like displacement from the top toward the bottom of the matrix. Behind the displacement front,

CO₂ vaporized the oil components and the rich-CO₂ phase replaced with the fresh CO₂ from the injector. The oil recovery behind the front is 100% at any time interval.

Effect of Injection Rate. An effort is made to investigate the effect of injection rate on the efficiency of the secondary-CO₂ injection into a base case matrix block surrounded by fractures. In many field applications under CO₂ injections, the main obstacle for successful CO₂-EOR project is the adverse effect of low injection rate that leads to unavailability of the fresh-CO₂ in the fracture in contact with the stagnant oil in the matrix. We consider several injection rates that result in $PV_{inj}=1$ at 2 years: $2.5E-04$ m³/day (*case a*), $PV_{inj}=1$ at 5 years: $9.9E-05$ m³/day (*case b*), $PV_{inj}=1$ at 10 years: $4.9E-05$ m³/day (*case c*), $PV_{inj}=1$ at 15 years: $3.3E-05$ m³/day (*case d*), $PV_{inj}=1$ at 30 years: $1.6E-05$ m³/day (*case e*), and $PV_{inj}=1$ at 50 years: $9.9E-06$ m³/day (*case f*). As shown by Fig. 14a, the high injection rate substantially increases the rate of oil recovery. For instance, the oil recovery jumps from less than 40% at 20 years in *case e* to 90% in *case a*. The *case a* may never exist because it requires significant number of injection wells and massive amount of CO₂ source.

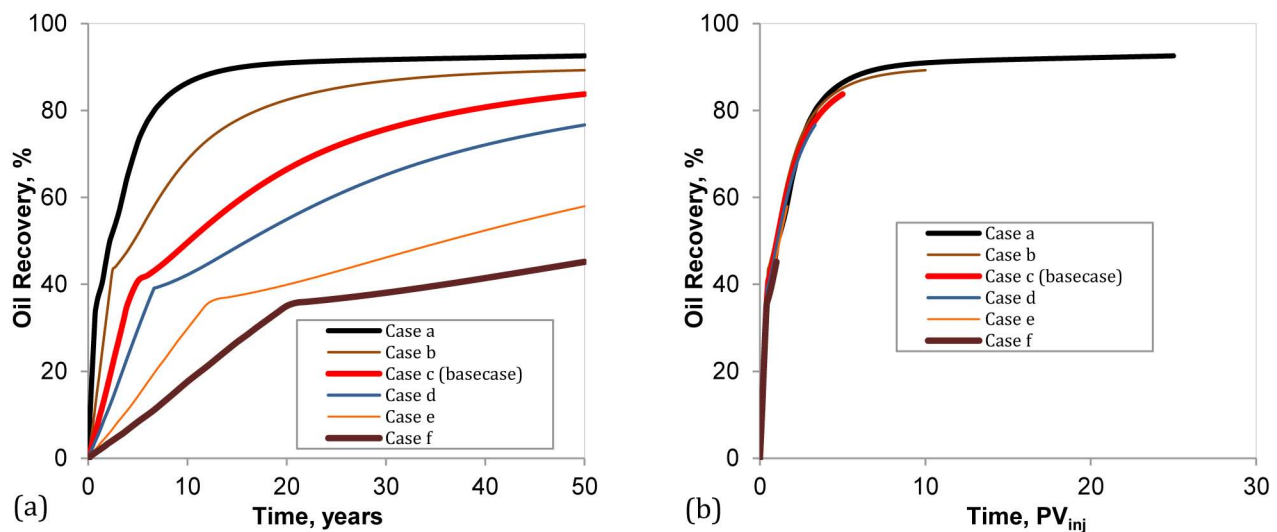


Figure 14—The oil recovery profile for cases a through f: (a) time basis, (b) PV_{inj} basis

Fig. 14b compares the effect of injection rate for oil recovery based on PV injected. The ultimate oil recovery for *all cases* is somehow similar at a particular PV_{inj} . However, the lower injection rate significantly delays the oil production. For instance, 60 % oil recovery is achieved for *case a* after 3.5 years of CO₂ injection, for case b after 7 years, for *case c* after 16 years, and case d after 25 years. The low injection rate for *case e* and *case f* results in poor efficiency of the CO₂-EOR in the field, the oil recovery never reaches to 60% during 50 years of CO₂ injections. Therefore, the integrated field optimization is required to obtain the require CO₂ amount to achieve the maximum efficiency of the CO₂-EOR during the prescribed years of the CO₂ injection in the field.

Effect of Injected gas. We study the effect of different injection gas compositions on the efficiency of the secondary gas injection into the base case model. In addition, with CO₂, the injected gases are C₁, N₂, and separator-gas. The current pseudoized EOS model provided by Ghasemi et al. (2016a and 2016b) has lumped C₁N₂ component. Employing the full EOS model provided by Ghasemi et al. (2016b), we redefine the pseudoized EOS with 11-components, providing separate C₁ and N₂ components in the characterization set. The diffusion coefficients for new 11-components EOS model is found by matching the result of Constant Volume Diffusion (CVD) experiment provided by Ghasemi et al. (2016.a).

Using the base case injection rate, Fig. 15 presents the efficiency of the secondary gas-flooding into a base case matrix surrounded by fractures. The ultimate oil recovery with diffusion for a 1m×1m×1m matrix

block is 84% for CO₂, 39% for Separator gas, 21% for C₁ and 6% for N₂. We observe that N₂ flooding has poorest efficiency for small block size and the role of diffusion is insignificant. The separator gas contains 20% intermediate components that results in higher diffusion effect and better efficiency compared with C₁ and N₂.

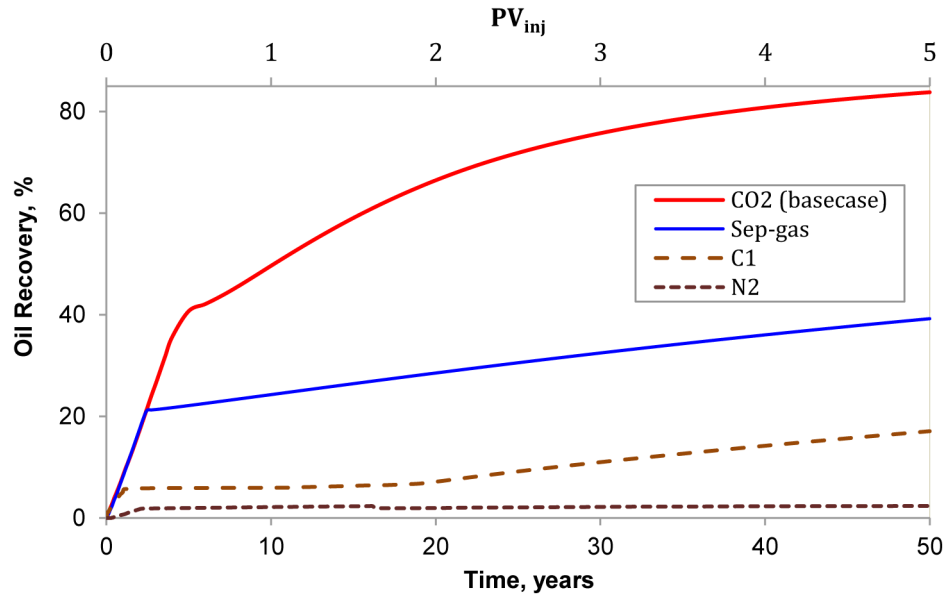


Figure 15—The performance of different injected gas on the oil recovery of the base case model.

The separator gas compositions changes during the life of the field, varying from minimum miscibility pressure (MMP) of ~417 bara to about 345 bara in which is still far from the CO₂ MMP of 207 bara. The source of CO₂ may be limited and insufficient for the injection purposes in the field. Therefore, the available CO₂ may be mixed with produced separator gas and reinjected into the reservoir. For this case, we evaluate the performance of gas injection subjected to different mixtures of CO₂ and the separator gas. Fig. 16 presents the results of the base case model for various amount of CO₂ in the CO₂/separator-gas mixtures, varying from 0-% to 100-% in the injected streams. We see that as amount of CO₂ increases, the efficiency of the process improves. Note that Fig. 16 may be different for the large block size where the gravity drainage mechanism is considerable.

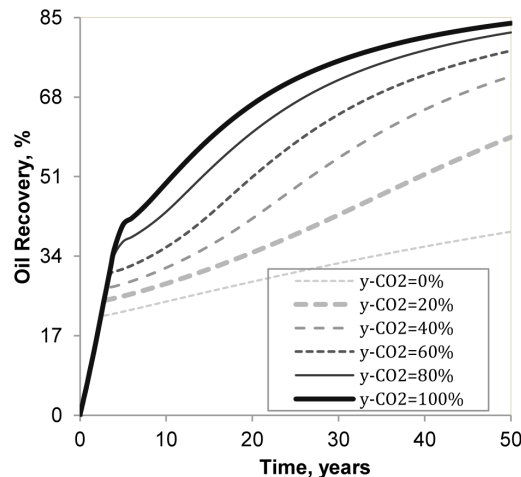


Figure 16—The performance of different CO₂/separator-gas mixtures on the oil recovery of the base case model.

Fig. 17 shows the effect of zero capillary pressure at three injection rates. We see that the oil recovery is significantly improved when no capillary force exists in the chalk matrix. The CO₂-gas breakthrough occurs at 10 years after 1 PV injection showing the piston like displacement developed under zero capillary pressure. Whereas the gas breakthrough time is much earlier for the base case model to be at 5 years.

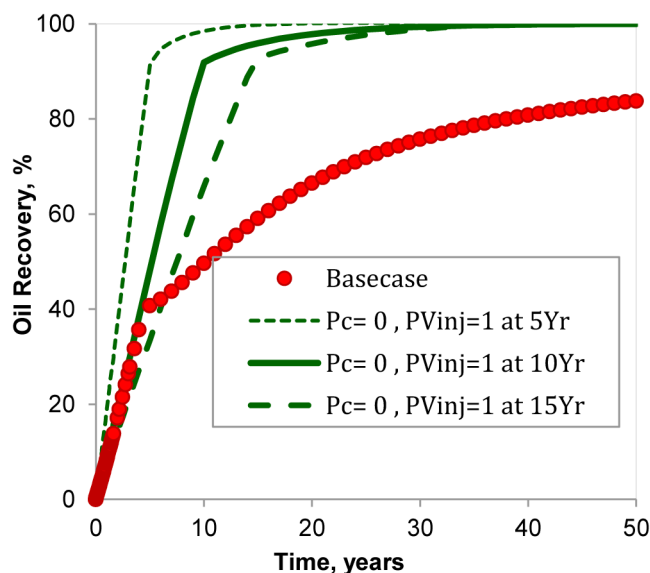


Figure 17—The Oil recovery profile after 50 years with zero capillary pressures and different injection rates. The solid red circle shows the basecase oil recovery

Effect of the Matrix Block Height and Fracture Spacing. In this section, we evaluate the effect of field-scale matrix block dimensions on the performance of secondary gas injection subjected to N₂, C₁ and CO₂. We consider the various fracture spacing (FS) of 0.5m, 1m, 5m, and 10m combined with several block heights (BH) of 100m, 10m, and 1m, covering the range of fracture spacing and block heights in the field. da Silva (1989) reports the average fracture spacing obtained from the core samples of initial vertical wells drilled in a NSCF reservoir. The data of fracture spacing are reported as a function of the fracture system permeability and ranges from 50 cm to 1 m at the most. In addition, we add wider range of fracture spacing from 50 cm to 10 m to evaluate their effect on the efficiency of the process. Moreover, wide range of block heights from 1m to 100m fluctuates the effect of diffusion and gravity drainage process acting as driving force against the capillary threshold. Table 3 provides 36 cases of the model results for the combination effect of fracture spacing, block heights and gas injection type. The injection rate is designed so that it provides $PV_{inj}=1$ after 10 years of gas injection for different size of matrix blocks. The total oil production and ultimate oil recovery are reported after 30 years ($PV_{inj}=3$) of gas injection scenarios.

TABLE 3—EFFECT OF BLOCK HEIGHT AND FRACTURE SPACING

Case	Injected Gas (I.G. ¹)	I.G. Rate ² , ×1000 res-m ³ /Day	Fracture Spacing, m	Block Height, m	I.G. ¹ /Prod. Oil, res-m ³ /S-m ³	Prod I.G. ¹ / Prod. Oil, S-m ³ /S-m ³	Prod-I.G. ¹ /Inj- I.G. ¹ , vol-%	Total Oil Production ³ , S-m ³	Oil Recovery (Ro) ³ , %
1	CO ₂	2.474	0.5	100	5.5	1152.5	69.6	4.89	80.74
2	CO ₂	0.247	0.5	10	4.7	953.0	67.3	0.58	95.14
3	CO ₂	0.025	0.5	1	5.9	1103.0	62.2	0.05	76.07
4	CO ₂	4.947	1	100	5.0	1027.6	69.2	10.92	90.07
5	CO ₂	0.495	1	10	4.6	940.1	67.2	1.17	96.31
6	CO ₂	0.049	1	1	5.9	1252.1	70.5	0.09	75.98
7	CO ₂	24.735	5	100	5.0	1021.2	68.1	54.18	89.4
8	CO ₂	2.474	5	10	4.7	948.5	67.2	5.79	95.49
9	CO ₂	0.247	5	1	6.0	1295.4	71.1	0.45	74.01
10	CO ₂	49.470	10	100	4.8	960.2	67.3	113.98	94.04
11	CO ₂	4.947	10	10	4.7	945.6	67.1	11.60	95.68
12	CO ₂	0.495	10	1	6.0	1214.1	67.4	0.91	37.45
13	C ₁	2.474	0.5	100	5.2	680.9	68.6	5.25	87.67
14	C ₁	0.247	0.5	10	5.2	695.7	69.4	0.52	87.06
15	C ₁	0.025	0.5	1	29.5	4614.8	81.0	0.01	15.31
16	C ₁	4.947	1	100	5.1	675.4	68.5	10.57	88.27
17	C ₁	0.495	1	10	5.2	700.9	69.3	1.03	86.24
18	C ₁	0.049	1	1	26.2	4114.7	81.4	0.02	17.27
19	C ₁	24.735	5	100	5.0	650.2	68.0	54.54	91.10
20	C ₁	2.474	5	10	5.2	695.3	68.9	5.18	86.46
21	C ₁	0.247	5	1	28.0	4980.8	92.2	0.10	16.15
22	C ₁	49.470	10	100	4.9	638.2	67.7	110.81	92.55
23	C ₁	4.947	10	10	5.2	687.9	68.7	10.44	87.17
24	C ₁	0.495	10	1	27.98	4381.2	81.2	0.19	16.17
25	N ₂	2.474	0.5	100	6.2	760.9	72.1	4.35	72.66
26	N ₂	0.247	0.5	10	7.4	1182.0	82.3	0.36	60.74
27	N ₂	0.025	0.5	1	89.3	13040.2	85.9	0.00	5.07
28	N ₂	4.947	1	100	6.1	743.4	71.9	8.87	74.10
29	N ₂	0.495	1	10	7.4	937.4	74.5	0.73	61.08
30	N ₂	0.049	1	1	62.6	9133.7	85.9	0.01	7.233
31	N ₂	24.735	5	100	5.2	608.3	69.2	52.27	87.32
32	N ₂	2.474	5	10	7.0	883.9	74.0	3.85	64.36
33	N ₂	0.247	5	1	84.6	12375.9	86.1	0.03	5.35
34	N ₂	49.470	10	100	5.0	583.2	68.6	108.15	90.32
35	N ₂	4.947	10	10	7.0	875.8	73.8	7.76	64.80
36	N ₂	0.495	10	1	82.2	11969.3	85.7	0.07	5.50

1. I.G. is for Injected Gas.
2. The all injection Gas rates result in P_{vinj}=1 after 10 years.
3. The oil recovery and total oil production are shown after 30 years.

For CO₂ flooding, the oil recovery is to be maximum for the case 5 with FS=1m and BH=10m. It may be due to maximum combination of gravity drainage and the diffusion process. The cost of project which determined by the amount of injected-CO₂ per volume of produced oil (I.G./Prod. Oil) is found to be minimum for case 5 and is 4.6 res-m³/S-m³. The diffusion alone process (BH=1m) contributes only to the maximum oil recovery of 76% that obtained to be for FS=0.5 (case 3). On the other word, when diffusion is dominant, the most effective block dimensions is with FS lower than 1 m and BH as low as 1m. Increasing the fracture spacing when block height is small will deteriorate the diffusion alone process and lead to low efficiency of the CO₂ flooding. For example, for BH=1m, the oil recovery drops significantly from 74% for FS=5m (case 9) to 37% for FS=10 m (case 12). Fig. 18 shows the rate oil of oil recovery for different fracture spacing at BH=1. Results show that the diffusion process is effective as long as the fracture spacing is around 5m or less. However, once the fracture spacing is larger than 5m recovery performance is significantly reduced. The average CO₂-recovery (defined as *produced-CO₂* divided by *injected-CO₂*) is found to be 67.9

% for all CO₂ cases. High CO₂ recovery facilitates the CO₂-EOR project to be less dependent to the main source of available CO₂ required for injection.

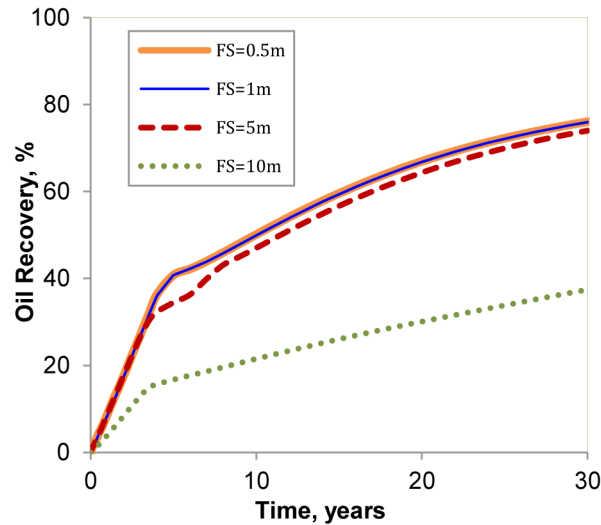


Figure 18—The oil recovery profile at BH=1m after 30 years (diffusive gas=CO₂)

N₂ and C₁ are found to be a promising gas injection in NSCF fracture reservoirs providing high efficiency for the block heights more than 10 m. The density difference that controls the rate of gravity drainage is higher for C₁ ($\Delta\rho_{og}=0.531$ g/cm³) and N₂ ($\Delta\rho_{og}=0.469$ g/cm³) compared with CO₂ ($\Delta\rho_{og}=0.153$ g/cm³) at NSCF reservoir conditions. The oil recovery for both C₁ and N₂ cases is maximum at the largest BH=100m and FS=10 m, resulting R_o=93% for C₁ (case 22) and R_o=90% for N₂ case (case 34). The average N₂- and C₁-recovery are 74% and 78% respectively. However, the efficiency of the N₂ and C₁ injection projects drop significantly for the matrix height below 10 m regardless of the different fracture spacing. In such cases the cost of the project increases significantly for instance the I.G./Prod. Oil ratio is 28 res-m³/S-m³ for C₁ and 78 res-m³/S-m³ for N₂.

Effect of S_w on Tertiary CO₂-Flooding. To evaluate the efficiency of the tertiary-CO₂ flooding, we inject CO₂ into a matrix block been initialized with the water saturation after secondary water flooding. We consider the $S_w=20\%$, 40% and 60% . The oil-water capillary pressure and relative permeability is provided by Ghasemi et al. (2017b) that represents moderate water wet system for the NSCF fractured reservoirs. We also update the diffusion coefficients for different water saturation considered in this study. Ghasemi et al. (2017b) show that the norm of diffusion coefficient ratio linearly decreases as the water saturation after water flooding is increased. This effect is mainly due to the fact that continuous water clusters do prevent the direct communication of the injected gas with the oil in the matrix. Hence area open for diffusion decreases which also reduces the effective diffusion coefficients. We evaluate the effect of S_w for different block height BH=1m and BH=20m and all at fixed FS=1m. Fig. 19 presents the plot of ultimate oil recovery after 20 years versus S_w -water flooding at the start of CO₂ injection. It reveals that for both block heights, the oil recovery is linearly decreased as the water flooding S_w increases. Moreover, the negative effect of water blockage is more notable for the small matrix block height.

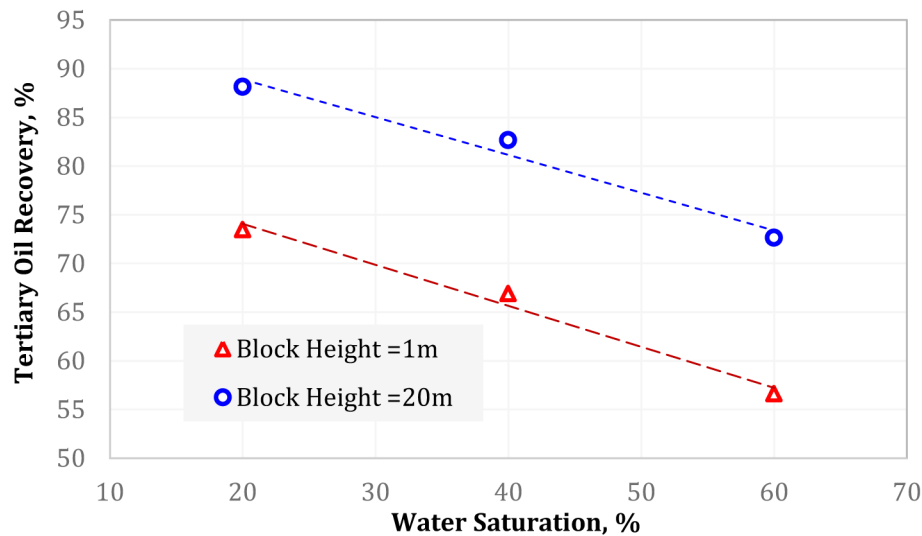


Figure 19—The Effect of water saturation after secondary WF on the performance of tertiary CO₂ flooding.

As shown by Fig. 19, the oil recovery changes from 90 % to 72% for BH=20m and from 73% to 60% for BH=1m, indicating the better performance of the CO₂ flooding in larger block heights. Note that the CO₂ solubility into aqueous phase is ignored in this study and it may have slightly negative effect on the performance of the process. The more solubility of CO₂ into the water, the less CO₂ is available to recover the oil, hence the current model slightly underestimates the real cost of the project (amount of injected-CO₂/Prod. Oil).

Accuracy of the Dual Porosity Models. Several dual porosity models together with their associated transfer functions are developed for a single-phase oil fractured reservoirs under active gravity drainage. Their accuracy is needed to be evaluated for different conditions under strong vaporization in the presence of diffusion (e.g. CO₂ injection), and weak vaporization using equilibrium gas injection. We compare the accuracy of the dual porosity models against the *accurate* single porosity model. We simplify the base case single porosity model to have matrix in direct contact with only one single vertical fracture eliminating the horizontal fractures at top and bottom of the block (Fig. 11c). This simplification allows to have mass-transfer between fracture and the matrix only through one side of the block, being more similar with the dual porosity models. Similar properties provided in four type of dual porosity models are compared with the single model (ECLIPSE 300-version 2012.1): (a) the normal dual porosity (*DP-1*) that assumes the matrix is the source and the oil can only be produced through high permeability fractures (Kazemi et al., 1976), (b) *DP-2* the dual porosity model described in (a) is equipped with a transfer function that takes into account the gravity and the imbibition between the matrix and the fracture cells, (c) *DP-3* the modified form of gravity drainage developed by Quandalle and Sabathier (1989), (d) *DP-4* the vertical discrete matrix gravity drainage model which consist of number of submatrix porosities connected to the fracture. The discrete model increases the resolution with height of the phase discontinuity and the gravitational potential. The shape factor used for all models is define based on Kazemi's formulation ($\sigma=4(1/(L_x^2+L_y^2+L_z^2))$) where L_x , L_y , and L_z are the matrix length in x,y, and z direction respectively.

Vaporization and Diffusion. We compare the results of DP models against SP model at different degree of vaporization together with or without molecular diffusion: *case a: no(or weak)-vaporization and no-diffusion* by injecting the equilibrium gas that has the incipient gas composition of the flashed oil at reservoir temperature and saturation pressure, *case b: moderate-vaporization and no-diffusion* by injecting N₁C₁ gas, *case c: strong-vaporization and no-diffusion*: by injecting CO₂ at high injections rate ($PV_{inj}=1$ at 2 years), and finally *case d: CO₂ injection with diffusion*.

Fig. 20a presents the accuracy of the DP models for *case a*. DP1, DP2 and DP3 over predict the oil recovery with maximum deviation of 320% for DP-2. The DP1 model results in better performance compared with DP2 and DP3. The best agreement can be found for DP-4 model with accurate prediction for oil recovery for the case with no-vaporization effect. The number of discrete matrix cells in DP-4 are two. We study the effect of number of matrix cells in DP-4 and the results were not affected by having higher number of sub-matrixes. As shown by Fig. 20b, the DP4 model in *case b* also results in good agreement. However, the quality of match for DP-4 model is slightly decreased. This is because the vaporization affects the phase distribution in the matrix which cannot be properly represented by the approximated transfer function defined in DP-4. The first three models still highly over-predict the oil recovery for case b. In *case c*, the effect of vaporization is strong and all DP models result in poor performance (Fig. 20c). Finally, when diffusion is on, *case d*, the DP-4 under predicts the oil recovery by ~10% (Fig. 20d).

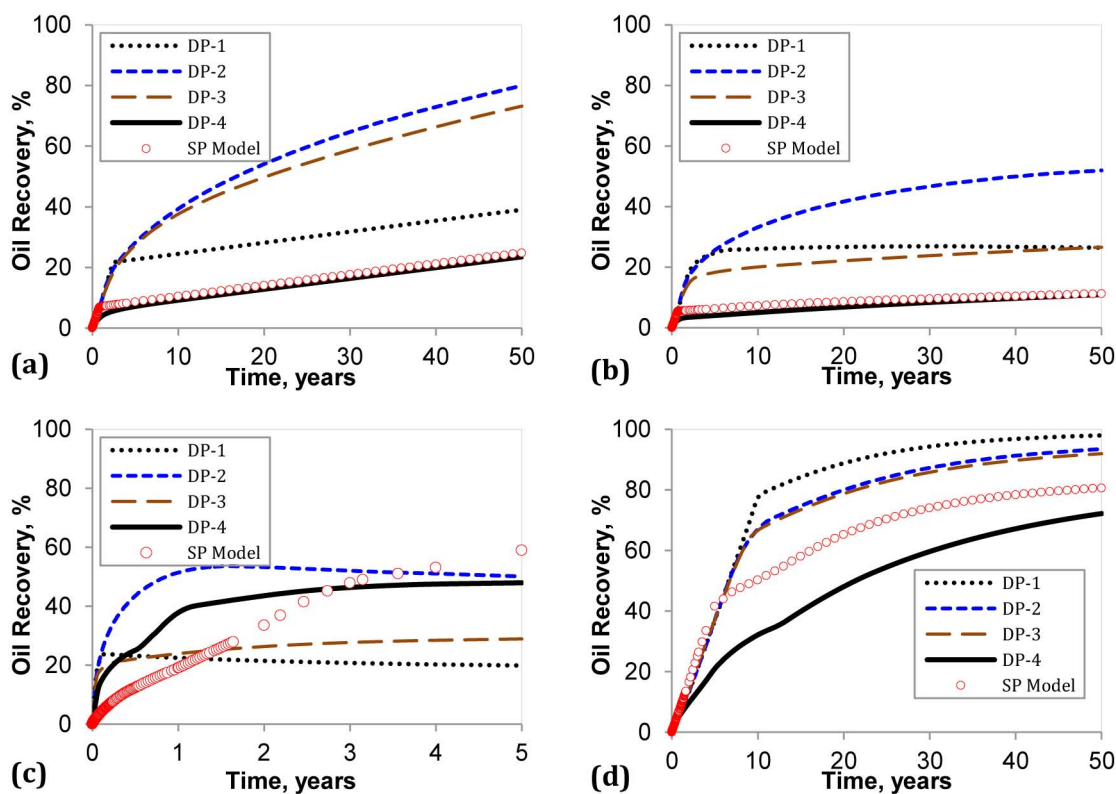


Figure 20—Accuracy of the dual porosity model at different condition: (a) case a, (b) case b, (c) case c, (d) case d

Block to Block Effect. We investigate the effect of re-infiltration using two, four and ten stack matrix blocks surrounded by fractures. The evaluation is first done using SP models including the effect of diffusion. In this example, the fracture network is more complex compared with the simple SP model described in Fig. 11C. Each single block ($1\text{m} \times 1\text{m} \times 1\text{m}$) is surrounded by horizontal and vertical fractures as depicted by Fig. 11d. Injector and producer are defined in the horizontal fracture located at the top and bottom of the model respectively. Then we test the accuracy of the DP models for all different configurations.

Fig. 21 shows that once miscibility is achieved, the infiltration has no considerable effect on the oil recovery for 2, 4 and 10 blocks. This is due to the fact that IFT between the gas and oil vanishes and hence the capillary forces diminish and no capillary imbibition takes place (Suicmez et al., 2011).

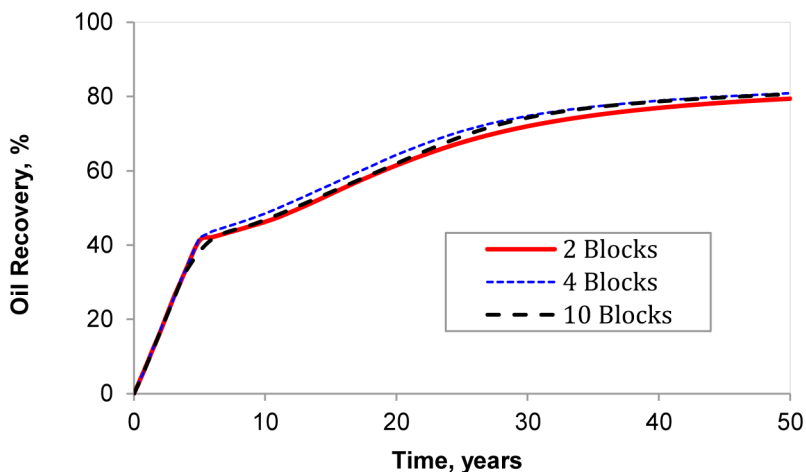


Figure 21—The effect of block-to-block on the performance of CO₂ flooding at the presence of diffusion

In general, all DP models described earlier, result in poor match performance and fail to mimic the main mass transport phenomena described by SP models presented for two and ten stack matrixes. For 4-stack matrix blocks, we observe that DP-3 results in good match as shown by Fig 22a. The quality of DP match can be improved by defining transmissibility multiplier (β) that activates the matrix-fracture connection between fracture grid block and the matrix grid block just below it. The multiplier adjusts the fractional contact between the upper fracture and the lower matrix. As shown by Fig. 22b, the accuracy of the 10-stacked matrix block under CO₂ injection with diffusion is improved by tuning the block-to-block multiplier. The best match transmissibility multiplier is found to be $\beta=0.3$ and results in better performance compared with a case when $\beta=0$.

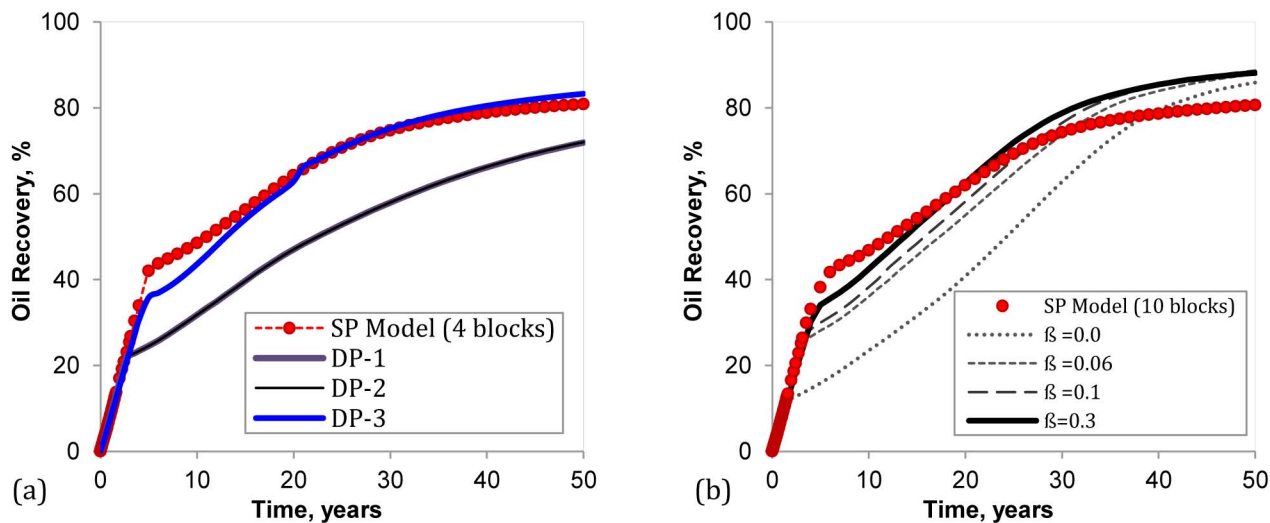


Figure 22—The accuracy of dual porosity models: (a) 4-stacked matrix blocks, (b) 10-stacked matrix blocks with/without block-to-block multipliers (β).

Therefore, the first step toward good practice of employing the DP models in full-field fracture reservoirs is to evaluate their accuracy against SP models in smaller scale. Their associated parameters such as sigma, type of transfer functions, block-to-block multipliers and other important parameters are required to be optimized to improve their accuracy under complex mass transport mechanisms.

Conclusion

Based on our modeling and experimental work, the main conclusions are:

1. We successfully conduct high pressure core flooding experiment that addresses the effect of pressure on the performance of tertiary-CO₂ flooding. The numerical modeling is capable of reproducing the experimental data for WF and CF period.
2. Our modeling shows Wood's Metal technique was successfully operated at reservoir condition during exchange process although the STO is not completely replaced by live-oil after the exchange process.
3. Strong spontaneous imbibition exists during the waterflooding which is due to the considerable amount of sulphate in the formation water. The final water saturation after WF was found to be very high at around 72%.
4. Diffusion coefficients are found to be important parameters affecting the recovery of tertiary-CO₂ flooding at high pressure conditions.
5. Hysteresis in capillary pressure and oil permeability are found to be important to match the water production before CO₂ flooding.
6. Our analysis shows that CO₂ flooding is more efficient at higher pressure. This is due to strong vaporization and viscosity reduction. For the operating conditions in this study, oil can dissolve up to more than 40% CO₂.
7. Modeling results on upscaling show that CO₂ flooding is a promising candidate for increasing oil recovery from different block heights ranging from 1 to 100 meters. However, its efficiency drops significantly for small matrix block height with large fracture spacing.
8. Injection rate accelerates the oil recovery as the ultimate oil recovery is found to be similar for different injection rates.
9. Methane and Nitrogen injection are found very efficient in increasing the oil recovery for block height more than 10 meters and fracture spacing ranging between 0.5m and 10m. However, the efficiency of the N₂ and C₁ flooding drops significantly when the matrix height is below 10 m regardless the size of the fracture spacing.
10. Accuracy of different dual porosity models are tested against the single porosity model. It is found that when the component exchange is negligible (the displacement is immiscible), dual porosity models may provide an acceptable accuracy. However, when the component exchange takes place and the diffusion is present none of the dual porosity models is able to match the single porosity representation.
11. For the block-to-block interaction, the accuracy of dual porosity model can be improved by employing transmissibility multiplier between matrix and neighboring fracture.

Acknowledgments

We would like to thank Joint Chalk Research (JCR) consortium for permission to publish this work and providing financial support of this study and series of other CO₂ EOR research projects in the North Sea. JCR consortium consists of Norwegian Petroleum Directorate (NPD), Danish Energy Agency, the Danish North Sea Fund, BP, ConocoPhillips, DONG, ENI, Hess, Maersk Oil, Shell, Statoil, and Total.

Nomenclatures

- D_g = gas diffusion coefficients, L²/t, cm²/hr
- D_o = oil diffusion coefficients, L²/t, cm²/hr
- N = number of grid cells
- p = pressure, m/Lt², bara
- P_c = capillary pressure, m/Lt², bara
- $P_{c,MAX}$ = maximum capillary pressure in the table, m/Lt², bara

- $P_{c,MIN}$ = minimum capillary pressure in the table, m/Lt², bara
 $P_{c,t}$ = capillary pressure at $S_{w,t}$, m/Lt², bara
 S_{or} = residual oil saturation, frac.
 S_{wir} = irreducible water saturation, frac.
 $S_{w,t}$ = water saturation at $P_{c,t}$, frac.
 T = temperature, T, °C

References

- Alavian, S.A. and Whitson, C.H. 2010. CO₂ EOS Potential in Naturally Fractured Haft Kel Field, Iran. *SPE Res Eval & Eng* **13** (04): 720–729. SPE-139528-PA. <http://dx.doi.org/10.2118/139528-PA>.
- Awan, A.R., Teigland, R., Kleppe, J. 2006. EOR Survey in the North Sea. Presented at the 2006 SPE/DOE Symposium on Improved Oil Recovery, USA, Oklahoma, Tulsa, 22-26 April. <https://doi.org/10.2118/99546-MS>.
- Bellveau, D., Payne, D.A., and Martin, M. 1993. Waterflood and CO₂ Flood of the Fractured Midale Field. *JPT* **45** (09). SPE-22946-PA. <http://dx.doi.org/10.2118/22946-PA>.
- da Silva, F.V. 1989. Primary and Enhanced Recovery of Ekofisk Field: A Single- and Double-Porosity Numerical Simulation Study. Presented at the 64th Annual Technical Conference and Exhibition of the Society of Petroleum Engineers, San Antonio, TX, USA. 8-11 October. SPE-19840-MS. <http://dx.doi.org/10.2118/19840-MS>.
- Enick, R.M., Olsen, D., Ammer, J. et al. 2012. Mobility and Conformance Control for CO₂ EOR via Thickeners, Foam, and Gels – A Literature Review of 40 Years of Research and Pilot Test. Presented at the Eighteenth SPE Improved Oil Recovery Symposium, Tulsa, Oklahoma, USA. 14-18 April. SPE-154122-MS. <http://dx.doi.org/10.2118/154122-MS>.
- Firoozabadi, A., Markeset, T.I. 1994. Miscible Displacement in Fractured Porous Media: Part I—Experiments. Presented at the SPE/DOE Ninth Symposium on Improved Oil Recovery, Tulsa, Oklahoma, U.S.A. 17-20 April. SPE-27723-MS. <http://dx.doi.org/10.2118/27743-MS>.
- Ghasemi, M., Astutik, W., Alavian, S. A., Whitson, C. H., Sigalas, L., Olsen, D., and Suicmez, V. S. 2016a. Determining Diffusion Coefficients for Carbon Dioxide Injection in Oil-Saturated Chalk by Use of a Constant-Volume-Diffusion Method, *SPE J. SPE-179550-PA*. doi:10.2118/179550-PA.
- Ghasemi, M., Astutik, W., Alavian, S. A., Whitson, C. H., Sigalas, L., Olsen, D., and Suicmez, V. S. 2016b. Lab Tests and Modeling of CO₂ Injection in Chalk with Fracture-Matrix Transport Mechanisms. Presented at SPE Europe featured at 78th EAGE Conference and Exhibition, Vienna, Austria, 30 May-2 June. SPE-180102-MS.
- Ghasemi, M., Astutik, W., Alavian, S. A., Whitson, C. H., Sigalas, L., Olsen, D., and Suicmez, V. S. 2017a. Experimental and Numerical Investigation of Tertiary-CO₂ Flooding in a Fractured Chalk Reservoir. Presented at the SPE Europe featured at 79th EAGE Annual Conference & Exhibition, Paris, France, 12-15 June. SPE-185869-MS.
- Ghasemi, M., Astutik, W., Alavian, S. A., Whitson, C. H., Sigalas, L., Olsen, D., and Suicmez, V. S. 2017b. Tertiary-CO₂ Flooding in a Composite Fractured-Chalk Reservoir. Presented at the SPE Reservoir Characterization and Simulation Conference and Exhibition, UAE, Abu Dhabi, 8-10 May. SPE-186946-MS.
- Ghedan, S. 2009. Global Laboratory Experience of CO₂-EOR Flooding. Presented at the 2009 SPE/EAGE Reservoir Characterization and Simulation Conference, USE, Abu Dhabi, 19-21 October. SPE-125581-MS. <https://doi.org/10.2118/125581-MS>.
- Goodyear, S.G., Koster, M.P., Marriott, K.A., et al. 2011. Moving CO₂ EOR Offshore. Presented at the SPE Enhanced Oil Recovery Conference, Kuala Lumpur, Malaysia, 19-21 July. <https://doi.org/10.2118/144939-MS>.
- Hoteit, H. and Firoozabadi, A. 2009. Numerical Modeling of Diffusion in Fractured Media for Gas Injection and Recycling Schemes. *SPE J.* **14** (2). SPE-103292-PA. <http://dx.doi.org/10.2118/103292-PA>.
- Jensen, T.B., Harpole, K. J., and Østhus, A. 2000. EOR Screening for Ekofisk. Presented at the SPE European Petroleum Conference, Paris, 24-25 October. SPE-65124-MS. <http://dx.doi.org/10.2118/65124-MS>.
- Karimaie, H. 2007. Aspects of Water and Gas Injection in Fractured Reservoir. PhD Dissertation, NTNU, Trondheim, Norway.
- Kazemi, H., Merrill, J.R., Porterfield, K.L., et al. 1976. Numerical Simulation of Water-Oil Flow in Naturally Fractured Reservoirs. *SPE J.* **16**(07). SPE-5719-PA. <https://doi.org/10.2118/5719-PA>.
- Martin, F.D. and Taber, J.J. 1992. Carbon Dioxide Flooding. *JPT* **44** (4): 396–400. SPE-23564-PA. DOI: 10.2118/23564-PA.
- Moortgat, J., Firoozabadi, A., and Li, Z. 2013. CO₂ injection in Vertical and Horizontal Cores: Measurements and Numerical Simulation. *SPE J.* **2**(18): 331–344. SPE-135563-PA. <http://dx.doi.org/10.2118/135563-MS>.
- Petroleumstreamz. 2015. Pipe-It User Manual, Version 1.5.2. Trondheim, Norway.
- Quandalle, P. and Sabathier, J.C. 1989. Typical Features of a Multipurpose Reservoir Simulator. *SPE J.* **16007** 4(04). SPE-16007-PA. <https://doi.org/10.2118/16007-PA>.

- Schlumberger. 2012. ECLIPSE 300 User Manual, Version 2012.1.
- Springer, N., and Korsbech, U., 2003, Resistivity Index Measurement Without The Porous Plate: A Desaturation Technique Based on Evaporation Produces Uniform Water Saturation Profiles and More Reliable Results for Tight North Sea Chalk, Presented at the International Symposium of the Society of Core Analysts held in Pau, France, 21-24 September 2003, SCA2003-38.
- Suicmez, V.S., Karpan, V., and Dindoruk, B.: 2011. Impact of Miscibility on Gas-Oil Gravity Drainage in Fractured Reservoirs, SPE Reservoir Characterization and Simulation Conference, Abu Dhabi, UAE.
- Tzimas, E., Georgakaki, A., Garcia, C.C., et al. 2005. Enhanced Oil Recovery Using Carbon Dioxide in the European Energy System. Report EUR 201895 EN.
- Zick Technology. 2015. PhazeComp User Manual, Version 1.8.1.
- Zuta, J., Ingebret, F., Roman, B., 2010. Experimental and Simulation of CO₂-Foam Flooding in Fractured Chalk at Reservoir Conditions: Effect of Mode of Injection on Oil Recovery. Presented at the SPE EOR Conference at Oil & Gas West Asia, Muscat, Oman, 11-13 April. SPE-129575-MS. <http://dx.doi.org/10.2118/129575-MS>.

Appendix A: The Developed EOS Model

Table A-1 provides the developed EOS model used in this study.

TABLE A-1—THE DEVELOPED EOS MODEL

Component	BIPs		M	T _c , K	p _c , bar	ω	s	T _b , K	γ	Z _{cvls}	Parachor
	N ₂ C ₁	CO ₂									
N ₂ C ₁	0.0000	0.0000	16.13	190.02	45.89	0.01113	-0.15008	111.27	0.14700	0.2862	70.91
CO ₂	0.1044	0.0000	44.01	304.12	73.74	0.22500	0.12009	184.89	0.76195	0.2743	34.73
C ₂	0.0001	0.1300	30.07	305.32	48.72	0.09900	-0.06280	184.44	0.32977	0.2792	111.00
C ₃	0.0003	0.1250	44.10	369.83	42.48	0.15200	-0.06381	230.93	0.50977	0.2763	151.00
C ₄ C ₅	0.0004	0.1160	63.00	436.32	36.04	0.21238	-0.04994	282.29	0.60368	0.2739	203.94
C ₆	0.0004	0.1150	81.60	514.07	34.52	0.23269	-0.00346	335.96	0.70906	0.2714	230.85
C ₇ C ₁₂	0.0284	0.0675	124.84	617.01	26.73	0.35753	0.05901	426.15	0.78814	0.2559	331.71
C ₁₃ C ₂₀	0.0440	0.0675	204.44	741.43	18.10	0.59290	0.16118	553.13	0.84830	0.2359	515.31
C ₂₁ C ₃₅	0.0586	0.0675	326.89	859.26	12.19	0.92018	0.24377	687.61	0.89692	0.2108	797.72
C ₃₆₊	0.0711	0.1522	563.64	926.04	11.24	1.30488	-0.08362	767.30	0.94986	0.1762	1343.76